

# A conservative SPH method for surfactant dynamics

S. Adami, X.Y. Hu, N.A. Adams

*Institute of Aerodynamics, Technische Universität München, 85748 Garching, Germany*

---

## Abstract

In this paper, a Lagrangian particle method is proposed for the simulation of multiphase flows with surfactant. The model is based on the multi-phase smoothed particle hydrodynamics (SPH) framework of Hu and Adams [1]. Surface-active agents (surfactants) are incorporated into our method by a scalar quantity describing the local concentration of molecules in the bulk phase and on the interface. The surfactant dynamics are written in conservative form, thus global mass of surfactant is conserved exactly. The transport model of the surfactant accounts for advection and diffusion. Within our method, we can simulate insoluble surfactant on an arbitrary interface geometry as well as interfacial transport such as adsorption or desorption. The flow-field dynamics and the surfactant dynamics are coupled through a constitutive equation, which relates the local surfactant concentration to the local surface-tension coefficient. Hence, the surface-tension model includes capillary and Marangoni forces. The present numerical method is validated by comparison with analytic solutions for diffusion and for surfactant dynamics. More complex simulations of an oscillating bubble, the bubble deformation in a shear flow, and of a Marangoni-force driven bubble show the capabilities of our method to simulate interfacial flows with surfactants.

*Key words:* SPH, Insoluble/soluble surfactant, Surface diffusion, Interfacial flow, Surface tension, Marangoni effects

---

## 1. Introduction

Multiphase systems occur in a wide range of technical or biological applications. The dynamics of such systems are much more complex than that of single-phase systems. Depending on the characteristic length scales, surface-tension forces at an interface may dominate inertia effects and thus have a strong influence on the overall flow evolution. Surface-tension effects can be differentiated into the capillary force and the Marangoni force. The former is proportional to the local curvature and minimizes the interface area, the latter accounts for surface-tension gradients along the interface.

Surface active agents (surfactants) offer the possibility to manipulate or even control the dynamics of multi-phase systems. By their nature, surfactant molecules adhere to a fluid interface and reduce the local surface tension as they form a buffer zone between the two phases. The surfactant at an interface is advected with the interfacial motion and may diffuse along the surface. Consequentially, surface-tension gradients can develop and influence the flow evolution. Besides the insoluble case, where all molecules are confined to the interface, the dynamics of the surfactant

can be coupled with the adjacent phases. Depending on the bulk concentration and the local interface concentration, adsorption and desorption may transport surfactant molecules between the bulk phase and the interface.

Surfactants are widely used in technical and biological applications. Due to the presence of surfactant, e.g. in a mixture of water and air, very small droplets can be formed which is useful to drug delivery, water purification and other applications. Even more important is the presence of surfactant in pulmonary alveoli, whose liquid-lining layer can function only with a substance that reduces surface tension (Pattle [2], Clements [3]). A simple estimate of the pressure in the liquid layer of an alveolar structure with a characteristic length scale of about  $100 \mu\text{m}$  and the Young-Laplace equation shows that a pure water-air interface ( $\sigma_0 \approx 0.07 \text{ N/m}$ ) would cause endexpiratory alveolar collapse and atelectasis (Von Neergard [4]). Moreover, surfactant molecules are believed to contribute also to pulmonary defence mechanisms and local immunomodulation (Hamm et al. [5]).

A numerical model describing interface dynamics including surfactants needs to handle the phase singularity at the interface and solve the surfactant evolution equation on the interface. Also, an evolution equation for the surfactant in the bulk solution needs to be coupled with the interfacial dynamics. As a consequence, the surfactant dynamics and the flow field cannot be solved independently from each other. Another important issue is the conservative formulation of the governing equations, in particular with respect to the mass of surfactant. These requirements render the modeling of multiphase flows with interfaces including surfactant effect a challenging task which has been studied already since about twenty years.

Early numerical investigations of the effect of surfactants in multiphase systems were limited to the insoluble case, where the transport of molecules between the bulk phase and the interface is neglected. The models were mainly used to investigate the effect of surfactants on drop deformation in a shear flow. Stone and Leal [6] solved the time-dependent convective-diffusion equation for surfactant transport on an interface using the boundary-integral method. While this work was restricted to two-dimensional problems, Yon and Pozrikidis [7] developed a fully three-dimensional finite volume method combined with the boundary-element method to study shear flows past a viscous drop. Whereas these methods described the interface in a discrete way, many following works used a continuous interface representation to account for interface dynamics. Xu and Zhao [8] used the Eulerian level set method, where the moving interface is formulated as zero level set on a Cartesian grid. They considered the interface to be convected passively by the flow, i.e. they prescribed the flow field and solved the surfactant dynamics on the interface without feedback to the flow field.

With respect to its importance for realistic long-time simulations and for accuracy reasons, the surfactant-mass conservation property was of special interest in subsequent works. James and Lowengrub [9] presented an fully coupled, axisymmetric, incompressible Navier-Stokes solver based on the "volume of fluid" (VOF) method and simulated insoluble surfactant dynamics on a moving interface. Different from previous works, they tracked the surfactant mass instead of solving the evolution equation for the concentration. Also, the surface area is tracked in this method instead of a reconstruction from the volume fraction. As consequence, for long-time simulations and strong interface deformations the reconstruction of the interface might be inconsistent with both the volume fraction and the surface area.

Xu et al. [10] used a level-set method for interfacial Stokes flows to investigate the effect of insoluble surfactants on single drops and droplet interactions. Conservation of surfactant material on the interface was enforced numerically by a rescaling operation, since the method itself was not formulated in conservative variables. Recently, Lai et al. [11] proposed an immersed-boundary method to simulate the interfacial problems with insoluble surfactant. Their main achievement is a new discretization for the surfactant concentration equation and a Lagrangian tracking of the interface, which allows for numerical conservation of the total mass of surfactant.

An important increase of considered complexity in the contaminated and moving interface problem was achieved by Zhang et al. [12]. They solved the fully coupled flow field and surfactant dynamics on the interface and in the bulk phase. The flux of surfactant on the interface was assumed to be balanced by adsorption and desorption. But this front-tracking method does not conserve the total mass of surfactant. Muradoglu and Tryggvason [13] also used the front-tracking method to simulate interfacial flows with soluble surfactant, but assumed that the mass transfer between the bulk phase and the interface occurs within a thin adsorption layer. They considered the axisymmetric-symmetric motion and deformation of a viscous drop moving in a circular tube and demonstrated first-order convergence of the surfactant mass error.

In this article, we present a numerical method that includes all main relevant surfactant dynamics in an incompressible Navier-Stokes solver based on the smoothed particle hydrodynamics (SPH) method. This Lagrangian formulation for multiphase problems requires no special interface capturing or tracking and can handle complex geometries as well as topology changes. We introduce the surfactant dynamics in conservative form and use mass fluxes to consider the exchange of surfactant between the interface and the bulk phase. Within the thin interface layer, we solve a diffusion equation for the surfactant, and due to our Lagrangian method advection is naturally included. Furthermore, we use different constitutive equations for the surface-tension correlation to demonstrate the general applicability of our method. We validate the method by comparisons with analytic solutions and grid convergence studies and show the exact conservation of surfactant mass on the interface and in the bulk phase. Finally, we study some complex multiphase problems such as the oscillating bubble experiment, the bubble deformation in shear flow and the Marangoni-force driven bubble.

In the next section, the governing equations for the flow field and the surfactant dynamics are presented, and the numerical algorithm summarizing also the main aspects of the SPH particle method is described in Section 3. The diffusion model in the bulk phase as well as on the interface and the coupling between them is validated and tested in Section 4. Some complex simulations are presented in Section 5 and finally, concluding remarks are given in Section 6.

## 2. Governing equations

The isothermal Navier-Stokes equations are solved in a moving Lagrangian frame

$$\frac{d\rho}{dt} = -\rho \nabla \cdot \mathbf{v} , \quad (1)$$

$$\frac{d\mathbf{v}}{dt} = \mathbf{g} + \frac{1}{\rho} [-\nabla p + \mathbf{F}^{(v)} + \mathbf{F}^{(s)}] , \quad (2)$$

where  $\rho$ ,  $p$ ,  $\mathbf{v}$ , and  $\mathbf{g}$  are material density, pressure, velocity and body force, respectively.  $\mathbf{F}^{(v)}$  denotes the viscous force and  $\mathbf{F}^{(s)}$  is the interfacial surface force.

In SPH, incompressible flow is usually modelled by the weakly-compressible approach, in which a stiff equation of state (EOS) is used to relate the pressure to the density, i.e.

$$p = p_0 \left( \frac{\rho}{\rho_0} \right)^\gamma + b , \quad (3)$$

with  $\gamma = 7$ , the reference pressure  $p_0$ , the reference density  $\rho_0$  and a parameter  $b$ . These parameters and the artificial speed of sound are chosen following a scale analysis presented by Morris et al. [14] which determines the threshold of the admissible density variation.

The viscous force  $\mathbf{F}^{(v)}$  then simplifies to the incompressible formulation

$$\mathbf{F}^{(v)} = \eta \nabla^2 \mathbf{v} , \quad (4)$$

where  $\eta$  is the dynamic viscosity. Following the continuum-surface-tension model (CSF), the surface force can be expressed as the gradient of the surface stress tensor with the surface tension coefficient  $\alpha$

$$\mathbf{F}^{(s)} = \nabla \cdot [\alpha (\mathbf{I} - \mathbf{n} \otimes \mathbf{n}) \delta_\Sigma] = -(\alpha \kappa \mathbf{n} + \nabla_s \alpha) \delta_\Sigma . \quad (5)$$

The Capillary force  $\alpha \kappa \mathbf{n} \delta_\Sigma$  is calculated with the curvature  $\kappa$ , the normal vector of the interface  $\mathbf{n}$  and the surface delta function  $\delta_\Sigma$ . This expression describes the pressure jump condition normal to an interface. In case of surface tension variations along the interface (e.g., due to non-uniform temperature or surfactant concentration) the Marangoni force  $\nabla_s \alpha \delta_\Sigma$  results in a tangential stress acting along the interface ( $\nabla_s$  is the surface gradient operator).

The evolution of surfactant on the interface is governed by an advection-diffusion equation with a source term accounting for the surfactant transport between the bulk and the phase interface, e.g. adsorption and desorption,

$$\frac{d\Gamma}{dt} = \nabla_s \cdot \mathbf{D}_s \nabla_s \Gamma + S_\Gamma , \quad (6)$$

where  $\Gamma$ ,  $\mathbf{D}_s$  and  $S_\Gamma$  are the interfacial surfactant concentration, the diffusion coefficient matrix (in case of isotropic

diffusion  $\mathbf{D}_s = D_s \cdot \mathbf{I}$ ) and the source term, respectively.

After integration over the domain, eq. (6) gives the variation of the total mass  $m_s$  of the interfacial surfactant

$$\frac{dm_s}{dt} = \frac{1}{dt} \int_V \Gamma \delta_\Sigma dV = \int_V \nabla_s \cdot \mathbf{D}_s \nabla_s \Gamma \delta_\Sigma dV + \int_V \dot{S}_\Gamma \delta_\Sigma dV. \quad (7)$$

The source term  $\dot{S}_\Gamma$  specifies the surfactant mass flux between the bulk phase and the interface. As widely used in the literature, the transport of surfactant is assumed to follow Langmuir kinetics (see Borwankar and Wasan [15])

$$\dot{S}_\Gamma = k_1 C_s (\Gamma^* - \Gamma) - k_2 \Gamma, \quad (8)$$

where  $k_1$  and  $k_2$  are the adsorption and desorption coefficients and  $C_s$  is the volumetric concentration of surfactant in the fluid phase immediately adjacent to the interface. The maximum equilibrium surfactant concentration is given by  $\Gamma^*$ .

Assuming that each surfactant molecule can move freely in the bulk phase, the transport of surfactant can be described by the advection-diffusion equation

$$\frac{dC}{dt} = \nabla D_\infty \nabla C. \quad (9)$$

Here,  $D_\infty$  denotes the bulk diffusion coefficient and  $C$  is the volumetric surfactant concentration in the liquid. After integration over the domain the rate of change of the total surfactant mass in the liquid  $M_s$  is obtained by

$$\frac{dM_s}{dt} = \int_V D_\infty \nabla^2 C dV - \int_V \dot{S}_\Gamma \delta_\Sigma dV. \quad (10)$$

The second term on the right side of eq. (10) is equal to the second term on the right hand side of eq. (7), hence ensures global mass conservation.

To close our model, we relate the interfacial surfactant concentration  $\Gamma$  to the surface-tension coefficient  $\alpha$  by a constitutive equation. In this paper, the model of Otis et al. [16] defined by two piecewise linear functions is used

$$\alpha(\Gamma) = \begin{cases} \alpha_0 + (\alpha^* - \alpha_0) \frac{\Gamma}{\Gamma^*}, & \Gamma \leq \Gamma^* \\ \alpha^* - \alpha_2 \left( \frac{\Gamma}{\Gamma^*} - 1 \right), & \Gamma^* < \Gamma \leq \Gamma_{max}. \end{cases} \quad (11)$$

In eq. (11),  $\alpha_0$  is the reference surface tension of the clean surface and  $\alpha^*$  is the reduced surface tension at the maximum equilibrium surfactant concentration  $\Gamma^*$ . The second part of the function is defined up to the maximum possible surfactant concentration  $\Gamma_{max}$  where the surface tension  $\alpha$  changes proportionally with factor  $\alpha_2$  to the non-dimensional concentration  $\Gamma/\Gamma^*$ . Note that the use of other relations, such as the Frumkin isotherm or the Langmuir model [12, 7, 17, 18], is straightforward.

The governing equations are nondimensionalized using reference values for the velocity  $u_0$ , the length scale  $l_0$ , the density  $\rho_0$  and the bulk concentration  $C_\infty$ . The non-dimensional characteristic numbers are

$$Re = \frac{\rho_0 u_0 l_0}{\eta}, \quad Ca = \frac{\eta u_0}{\alpha_0}, \quad Bo = \frac{\rho g l_0^2}{\alpha_0}, \quad (12)$$

$$Pe_s = \frac{u_0 l_0}{D_s}, \quad Pe_\infty = \frac{u_0 l_0}{D_\infty}, \quad Da = \frac{\Gamma^*}{C_\infty l_0}, \quad (13)$$

where  $Re$ ,  $Ca$ ,  $Bo$ ,  $Pe_s$ ,  $Pe_\infty$  and  $Da$  are the Reynolds number, the capillary number, the Bond number, the Peclet number based on  $D_s$ , the Peclet number based on  $D_\infty$  and the Damköhler number [13].

### 3. Numerical method

The governing equations are discretized using the multi-phase SPH method of Hu and Adams [1]. Each particle represents a Lagrangian element of fluid, carrying all local phase properties. With updating the positions of the particles, this method accounts for advection as the governing equations are formulated in terms of material derivatives.

#### 3.1. Multi-phase flow solver

According to Hu and Adams [1], we calculate the density of a particle  $i$  each timestep from a summation over all neighboring particles  $j$

$$\rho_i = m_i \sum_j W_{ij} = \frac{m_i}{V_i}. \quad (14)$$

Here,  $m_i$  denotes the particle mass,  $W_{ij} = W(\mathbf{r}_i - \mathbf{r}_j, h)$  is a kernel function with smoothing length  $h$  and  $V_i$  is the volume of particle  $i$ . Based on the studies of Morris et al. [14], we use the quintic spline function. This summation allows for density discontinuities and conserves mass exactly.

The pressure term in the momentum equation is approximated as

$$\frac{d\mathbf{v}_i^{(p)}}{dt} = -\frac{1}{\rho_i} \nabla p_i = -\frac{1}{m_i} \sum_j (V_i^2 p_i + V_j^2 p_j) \frac{\partial W}{\partial r_{ij}} \mathbf{e}_{ij}, \quad (15)$$

with the weight-function gradient  $\frac{\partial W}{\partial r_{ij}} \mathbf{e}_{ij} = \nabla W(\mathbf{r}_i - \mathbf{r}_j)$ . Note that this form conserves linear momentum exactly since exchanging indices  $i$  and  $j$  in the sum leads to an opposite pressure force. The viscous force is derived from the inter-particle-averaged shear stress with a combined viscosity. A simplification for incompressible flows gives

$$\frac{d\mathbf{v}_i^{(v)}}{dt} = \nu_i \nabla^2 \mathbf{v}_i = \frac{1}{m_i} \sum_j \frac{2\eta_i \eta_j}{\eta_i + \eta_j} (V_i^2 + V_j^2) \frac{\mathbf{v}_{ij}}{r_{ij}} \frac{\partial W}{\partial r_{ij}}, \quad (16)$$

where  $\nu_i = \eta_i / \rho_i$  is the local kinematic viscosity of particle  $i$ ,  $\mathbf{v}_{ij} = \mathbf{v}_i - \mathbf{v}_j$  is the relative velocity of particle  $i$  and  $j$  and  $r_{ij} = |\mathbf{r}_i - \mathbf{r}_j|$  is the distance of the two particles.

The calculation of the interface curvature to determine the surface tension can be avoided. For this purpose, in the continuous surface force model (CSF) the surface force is rewritten as the gradient of a stress tensor. The gradient of the color function  $c_i$  is used as approximation of the surface delta function  $\delta_\Sigma$ . This color function defines to which phase particle  $i$  belongs, i.e.  $c_i = 0$  for phase 1 and  $c_i = 1$  for phase 2. Since this function has a unit jump at the phase interface, the particle averaged gradient  $\nabla c_i$  of particle  $i$

$$\nabla c_i = \frac{1}{V_i} \sum_j \left[ V_i^2 c_i + V_j^2 c_j \right] \frac{\partial W}{\partial r_{ij}} \mathbf{e}_{ij} \quad (17)$$

has a delta-function-like distribution. Hence, the interface stress between phase 1 and 2 is obtained as

$$\Pi_i^{(s)} = \alpha_i \frac{1}{|\nabla c_i|} \left( \frac{1}{d} \mathbf{I} |\nabla c_i|^2 - \nabla c_i \nabla c_i \right), \quad (18)$$

where  $d$  denotes the spatial dimension and  $\alpha$  is the surface tension coefficient between the phases 1 and 2. Finally, the particle-averaged gradient of this stress term gives the particle acceleration due to surface tension

$$\frac{d\mathbf{v}_i^{(s)}}{dt} = \frac{1}{m_i} \sum_j \frac{\partial W}{\partial r_{ij}} \mathbf{e}_{ij} \cdot \left( V_i^2 \Pi_i^{(s)} + V_j^2 \Pi_j^{(s)} \right). \quad (19)$$

### 3.2. Surfactant kinetics

Using the color function to distinguish different phases in the system, particles with a non-vanishing color-function gradient approximate the singularity at an interface as a narrow transition band, see Fig. 1.

[Figure 1 about here.]

Within this narrow band of particles, the governing equations for the interfacial phenomena (6) - (8) are solved locally for each individual particle. Hence, using the color-gradient function as surface-delta function, an interfacial particle  $i$  contributes to the interface area by

$$A_i = V_i |\nabla c_i| \quad (20)$$

(in two dimensions,  $A_i$  and  $V_i$  are the interface length and the particle area). Corresponding to the individual interface area fraction, each particle carries a fraction of interfacial mass of surfactant  $m_{si}$ . The evolution of the surfactant mass fraction of a single particle due to adsorption and desorption is given by

$$\frac{dm_{si}^{(s)}}{dt} = S_{\Gamma_i} A_i = \left[ k_1 C_\infty (\Gamma^* - \Gamma_i) - k_2 \Gamma_i \right] A_i, \quad (21)$$

where the subscript ( $s$ ) indicates the effects due to adsorption and desorption. To assure the numerical stability for particles with small interface area, the interfacial surfactant concentration is calculated from a kernel average

$$\Gamma_i = \frac{\sum_j m_{sj} W_{ij}}{\sum_j A_j W_{ij}}, \quad (22)$$

where summation is on all neighboring interface particles, i.e. all neighboring particles which are within the narrow transition band.

As we solve the surfactant equations in conservative form, the total mass of surfactant is conserved exactly. Due to particle motion it may happen, that interface particles leave the transition band and transport surfactant material away from the interface. In that case, the interfacial surfactant mass of this escaped particle is mapped back to the remaining interface particles, see Appendix A.

### 3.3. Bulk diffusion

The diffusion in the bulk phase has a similar form as the viscous force in the momentum equation for an incompressible flow. Hence, the SPH approximation of the diffusion equation in conservative form follows in analogy to eq. (16) as

$$\frac{dM_{si}}{dt} = \sum_j \frac{2D_{\infty i} D_{\infty j}}{D_{\infty i} + D_{\infty j}} (V_i^2 + V_j^2) \frac{C_{ij}}{r_{ij}} \frac{\partial W}{\partial r_{ij}}, \quad (23)$$

where  $M_{si}$  is the mass of surfactant in the bulk phase of particle  $i$ ,  $D_{\infty i}$  and  $D_{\infty j}$  are the bulk diffusion coefficients of particle  $i$  and  $j$  and  $C_{ij} = C_i - C_j$  is the concentration difference. Note that the average diffusion coefficient in eq. (23) ensures the zero-flux condition between two phases if one diffusion coefficient is zero. Each time step, after updating the particle surfactant mass and particle volume, the local bulk concentration is calculated from

$$C_i = \frac{M_{si}}{V_i}. \quad (24)$$

### 3.4. Interfacial diffusion

Following Bertalmío et al. [19], the interfacial diffusion equation (6) can be expressed as

$$\frac{d\Gamma}{dt} = \nabla_s \cdot \mathbf{D}_s \nabla_s \Gamma = \frac{1}{|\nabla c|} \nabla \cdot [\mathbf{P}_s \mathbf{D}_s \nabla \Gamma |\nabla c|], \quad (25)$$

where  $\mathbf{P}_s = \mathbf{I} - \mathbf{n} \otimes \mathbf{n}$  is the operator, which projects the gradient of the surfactant concentration  $\nabla \Gamma$  tangentially to the interface (i.e. the surface gradient operator  $\nabla_s \Gamma$ ). This formulation solves the interfacial diffusion on a surface of a finite width and thus is well suited for the interfacial modelling within the smoothed particle hydrodynamics framework.

Discretizing eq. (25) with SPH, we calculate the term in the brackets on the RHS ( $\lambda = \mathbf{P}_s \mathbf{D}_s \nabla \Gamma |\nabla c|$ ) for each particle and use the general SPH summation formula to calculate the divergence of  $\lambda$ . Finally, the material derivative



of the interfacial surfactant mass fraction by interfacial diffusion is

$$\frac{dm_{si}^{(d)}}{dt} = \sum_j (\lambda_i V_i^2 + \lambda_j V_j^2) \frac{\partial W}{\partial r_{ij}} \mathbf{e}_{ij}. \quad (26)$$

Particles on the fringes of the interface transition band might have only one neighboring particle of a different phase. Hence, the simple normalized color gradient could lead to a wrong approximation of the interface normal direction. As a remedy, we calculate the normal vector by a weighted summation of the color gradients of the interfacial neighbors  $j$

$$\mathbf{n}_i = \frac{\sum_j \nabla c_j A_j}{|\sum_j \nabla c_j A_j|}. \quad (27)$$

Here, the interfacial area fraction  $A_j$  is used as weighing factor since the color gradient of the interface nearest particle is a better approximation of the normal direction (see Sec. 4.2, Fig. 4(b)).

As a consequence of the finite transition region, the general SPH discretization does not everywhere give an accurate estimate of the surfactant gradient. The neighbors of a particle adjacent to the interface do not all belong to the interface and must therefore be excluded from the gradient calculation. Following Chen et al. [20], a corrected gradient calculation at position  $\mathbf{x}_i$  yields

$$\nabla \Gamma(\mathbf{x}_i) = \left[ \sum_j (\mathbf{x}_i - \mathbf{x}_j) V_j^2 \nabla W_{ij} V_j \right]^{-1} \cdot \sum_j (\Gamma_i - \Gamma_j) V_j^2 \nabla W_{ij} V_j. \quad (28)$$

This formulation is valid for all situations where a particle has at least two neighbors. The implementation of eq. (28) is for both two and three dimensions straightforward since only a  $d \times d$  matrix inversion has to be performed.

During time integration, due to particle motion in the transition band around the interface a non-uniform and non-smooth surfactant concentration profile normal to the interface may develop. In the limit of an infinitely high resolution, this unphysical effect vanishes as the width of the transition region tends to zero. Nevertheless, to increase the accuracy especially for lower resolution simulations, we introduce a smoothing of the surfactant concentration normal to the interface. Instead of using a reinitialization as presented by Sbalzarini et al. [21], we adopt the directed-diffusion approach to introduce artificial normal diffusion within the transition band. For this purpose, eq. (25) is extended with the artificial normal diffusion as

$$\frac{d\Gamma}{dt} = \nabla_s \cdot \mathbf{D}_s \nabla_s \Gamma = \frac{1}{|\nabla c|} \nabla \cdot [\mathbf{P}_s \mathbf{D}_s \nabla \Gamma |\nabla c| + \mathbf{P}_n \mathbf{D}_n \nabla \Gamma |\nabla c|], \quad (29)$$

where  $\mathbf{P}_n = \mathbf{n} \otimes \mathbf{n}$  and  $\mathbf{D}_n = D_n \mathbf{I}$  are the normal projection matrix and the normal diffusion coefficient matrix.

### 3.5. Coupling between the bulk phase and the interface

The evolution of surfactant on the interface and in the bulk phase is coupled by the source term  $\dot{S}_\Gamma A$ , thus global conservation of mass is ensured. If one fluid phase is insoluble for surfactant but has an interface containing surfac-

tant, a special treatment of its interface particles is needed. Physically, the bulk surfactant concentration  $C_k$  and the interfacial surfactant concentration  $\Gamma_k$  of such a particle  $k$  are zero. But as these particles contribute to the surfactant dynamics within the transition band, the bulk concentration must be extrapolated from the interface particles of the adjacent phase. Accordingly, the calculated surfactant mass flux of these particles must be taken into account on the opposite bulk particles. The mathematical formulation of this coupling is given in Appendix B.

### 3.6. Time-step criteria

The equations presented above are integrated in time with an explicit predictor - corrector scheme. All quantities are updated in every substep. For stability reasons the maximum time step is chosen based on several time-step criteria [22, 23], see Appendix C.

## 4. Validation

To validate our modeling and implementation of the diffusion effects and surfactant kinetics with SPH we consider several two-dimensional test cases isolating each single effect. Provided that an analytic solution is available, we compare our results and test for convergence.

### 4.1. Bulk diffusion

In a first test we calculate the diffusion of a scalar species in a bulk liquid phase. For the computational domain we choose a square of fluid surrounded by solid walls with a length of  $l_x = l_y = 0.1 \text{ m}$  in each direction. The diffusion coefficient of the liquid phase is taken to be  $D = 4 \cdot 10^{-6} \text{ m}^2/\text{s}$ . Using an initial exponential distribution of the concentration field  $C(x, t)$

$$C(x, t = 0) = \exp\left[\frac{-(x - x_0)^2}{4DT_0}\right], \quad (30)$$

the analytic solution of the diffusion problem follows from

$$C(x, y, t) = \frac{A}{\sqrt{t + T_0}} \exp\left[\frac{-(x - x_0)^2}{4D(t + T_0)}\right], \quad (31)$$

where  $T_0 = 1 \text{ s}$ ,  $A = 1 \text{ kg m}^{-3} \text{ s}^{1/2}$  and  $x_0 = l_x/2$ .

[Figure 2 about here.]

Fig. 2(a) shows the evolution of the concentration profiles at  $t = 1.5$  and  $3$ . The solid lines represent the exact analytic solution and the symbols denote the results of a simulation with smoothing length  $h = 8.3 \cdot 10^{-3}$ . Even though this resolution is relatively poor, the calculated profiles are in very good agreement with the analytic solution. To evaluate the accuracy of our calculation quantitatively we define the error norm  $L_1$

$$L_1 = \frac{\sum_j |C_j - C(x_j, t)|}{\frac{C_{\infty} N}{10}}, \quad (32)$$

which is the normalized particle averaged deviation from the analytic solution. Here,  $N$  denotes the total number of particles. In Fig. 2(b) the error norm  $L_1$  is plotted with respect to the smoothing length  $h$ . As expected, with increasing resolution the error decreases and converges approximately with second order.

#### 4.2. Surface diffusion

For validation of the surface diffusion model we calculate the temporal evolution of an initially non-uniformly distributed surfactant concentration profile on an interface. We put a drop with radius  $R = 1 \cdot 10^{-3} \text{ m}$  into a liquid environment (centered in a Cartesian coordinate system) and initialize the interfacial surfactant concentration with the solution from Xu et al. [8] at  $t = 0$

$$\Gamma(\Theta, t) = \frac{\Gamma_\infty}{2} [\exp(-t) \cos(\Theta) + 1] . \quad (33)$$

Here,  $\Theta$  is the counterclockwise angle of the interface with respect to the x-axis.

[Figure 3 about here.]

Fig. 3(a) shows the prediction of the interfacial concentration profiles with our SPH-model compared to the analytic solution at several timesteps. The calculations were performed with a dimensionless smoothing length  $h = 0.5$ , a surface diffusivity of  $D = 1 \cdot 10^{-6} \text{ m}^2/\text{s}$  for both the tangential and normal diffusion and a maximum surfactant concentration  $\Gamma_\infty = 3 \cdot 10^{-6} \text{ kg/m}^2$ . The calculated profiles only show very small discrepancies from the analytic solution. These errors converge with about first order, see Fig. 3(b).

To clarify the influence of the interface-normal approximation, in a next step we neglect the diffusivity on the interface ( $D_s = 0 \text{ m}^2/\text{s}$ ) and simulate the surfactant concentration evolution on a steady air-water interface. Physically, the profile is expected to remain at the initial condition. The left profile in Fig. 4(a) shows the surfactant profile after  $t = 5$  using the normalized color gradients as normal direction  $\mathbf{n}_i = \nabla c_i / |\nabla c_i|$ . The profile is not smooth and differs strongly from the initial condition. This problem arises from the fact, that the particles are initially positioned on a Cartesian grid and the that circular interface is not represented accurately. Consequently, the color gradients do not represent the correct normal direction, which is shown in the left plot of Fig. 4(b). Note that the length of the vectors is adjusted for clarity.

We solved this problem with the introduction of the averaged normal calculation with eq. (27). The corresponding surfactant profile and normals are shown in the right plots in Fig. 4(a) and 4(b). The initial surfactant profile is preserved and the normal diffusion does not introduce artificial surface diffusion.

[Figure 4 about here.]

#### 4.3. Surfactant kinetics

Now we test our implementation of the interfacial surfactant transport and the coupling between the bulk phase and the interface. For this purpose, the adsorption of surfactant molecules to an initially clean interface is investigated.

A bubble of size  $R = 1 \cdot 10^{-3}m$  is exposed to a liquid phase with a constant surfactant concentration of  $C(x, t = 0) = C_0 = 1kg/m^3$ .

Assuming the bulk phase to be very large and the diffusion process to be infinitely fast, the bulk surfactant concentration directly underneath the interface is constant. Thus, from eq. (8) using the parameters  $k_1 = 1 kg/m^3/s$ ,  $k_2 = 0.1 \cdot 1/s$  and  $\Gamma^* = 0.005 kg/m^3$  an equilibrium surfactant concentration can be obtained as

$$\frac{\Gamma_{eq}}{\Gamma^*} = \frac{k_1 C}{k_1 C + k_2} \approx 0.91, \quad (34)$$

where the adsorption and desorption rates balance each other, and the surfactant concentration remains constant. The first line in Fig. 5(a) shows the result of a simulation of a fixed air bubble in a surfactant-rich water surrounding ( $1 : D_\infty = \infty$ ). As a reference, the broken horizontal line shows the analytic equilibrium state.

[Figure 5 about here.]

Now we include diffusion effects, i.e. the surfactant kinetics from eq. (8) depend also on the local volume concentration of surfactant at the interface  $C_{r=R}$ . The diffusion coefficient in the bulk liquid phase is set to  $D_\infty = 1 \cdot 10^{-6}m^2/s$ , which corresponds to a Peclet number of  $Pe_\infty = 0.1$  (using the velocity scale  $u_\infty = l_\infty k_2$ ). The second line in Fig. 5(a) shows the evolution of the interfacial surfactant concentration including the coupling with the liquid phase ( $2 : D_\infty = 10^{-6}m^2/s$ ). The corresponding evolution of the bulk concentration in the subsurface region directly underneath the interface is also plotted in this figure ( $3 : C_{r=R}, D_\infty = 10^{-6}m^2/s$ ). Since the adsorbed surfactant material is taken from the liquid phase, the bulk concentration  $C_{r=R}$  decreases, and at the same time the interfacial concentration  $\Gamma$  does not increase as fast as in the infinite diffusion case. From  $t \approx 2$  the bulk concentration increases again, caused by diffusion of surfactant in the liquid phase and a reduced surfactant flux between the interface and the bulk phase. The evolution of surfactant mass on the interface and in the liquid phase over time is shown in Fig. 5(b). As can be expected, with an increasing surfactant mass on the interface the surfactant mass in the liquid phase decreases. The total amount of surfactant in the system is conserved.

## 5. Results and discussion

With the results presented above we have shown the validity and accuracy of our model. In the following, we perform more complex two-dimensional simulations with coupled effects.

### 5.1. Oscillating bubble

Following Otis et al. [16], we simulate the dynamic surface tension of an air-water-like interface with surfactant. As in this problem the densities of the two phases do not determine the evolution, we assume the "air" and "water" phase to have a density ratio of 10 only to facilitate computation. The viscosities of the two phases are chosen such

that the ratio of the kinematic viscosities is comparable to the realistic case. Due to this smaller density difference, we avoid too small timesteps and decrease the computational time, see Hu and Adams [1].

As in the experiment, an air bubble is exposed to a liquid environment containing surfactant molecules. Enforcing an oscillation of the bubble, the dynamics of the surfactant transportation can be investigated. In our SPH method we perform the bubble oscillation by changing the mass of the air particles. This resembles the blowing and suction of air in the experiment. Consequently, the density of the particles changes and the pressure force drives the bubble to change its size. Starting from a droplet with initial radius of  $r_{max} = 0.02 \text{ m}$  at an equilibrium surfactant concentration  $\Gamma^* = 3 \cdot 10^{-6} \text{ kg/m}^2$ , the size of the air-water interface is oscillated sinusoidally with the period  $T$  and the evolution of the surfactant concentration on the interface is calculated. In the first set of simulations we assume adsorption-limited surfactant dynamics. Thus the bulk surfactant concentration is constant since the diffusion in the liquid phase is considered to be infinitely fast. The surfactant dynamics from eq. (8) are extended to the insoluble and the squeeze-out regime, see Otis et al. [16]. In the second regime ( $\Gamma^* \leq \Gamma < \Gamma_{max}$ ) the interface is insoluble, i.e. the concentration changes only by interface deformation,

$$\frac{dm_s}{dt} = \frac{d(\Gamma A)}{dt} = 0. \quad (35)$$

Reaching the maximum surfactant concentration  $\Gamma_{max}$ , the surfactant molecules are packed as tightly as possible in the interface and further compression results in an squeeze-out of molecules back to the bulk phase.

Figure 6(a) shows the surface-tension loops for various adsorption depths  $\tilde{k} = k_1 C / k_2$  at a Biot number of  $Bi = k_2 T = 1$  for the adsorption-limited case. At a very low adsorption depth the minimum possible surface tension is never reached during an oscillation cycle. This is due to the fact, that in the bulk phase there are not enough surfactant molecules available to accumulate at the interface. Increasing the adsorption depth, this limit is overcome and the nearly-zero surface tension occurs in the loop. Furthermore, the hysteresis increases with increasing adsorption depth.

[Figure 6 about here.]

Morris et al. [24] showed that under some conditions "pseudo-film collapse" occurs in the dynamic surface tension loops. Similarly to the true film collapse at the lowest possible surface tension, in this case the surface tension remains relatively constant near the equilibrium  $\alpha^*$  even though the interface is further compressed. As they showed in their experiments, this is not a numerical artifact but a physically realistic behavior. Following the experimental investigations, we have checked if our model recovers this phenomenon correctly. A variation of the Biot number at a fixed adsorption depth is given in Fig. 6(b). As seen in the experiments, with increasing Biot number the maximum occurring surface tension within the loop decreases. At very high desorption rates the "pseudo-film collapse" is observed.

Comparisons with experiments have shown, that under certain conditions the adsorption-limited model tends to predict a wrong transient behavior, i.e. the assumption of a constant bulk surfactant concentration does not hold in all situations. As a remedy, Morris et al. [24] consider the diffusion-limited surfactant dynamics. With this model

they are able to reproduce the experimental observations of Schürch et al. [25] and get even better agreement with the steady-state oscillations than with the adsorption-limited model. Using eq. (7) and (10), we can simulate with our SPH method the fully coupled interfacial surfactant dynamics with the bulk diffusion. As an example, Fig. 7 shows the concentration evolution in the bulk subsurface region directly underneath the interface and the surface-tension loop for the dynamic cycling with the parameters  $Bi = 10$ ,  $\tilde{k} = 10$ ,  $Da = 1$  and  $Pe = 1$ . Due to the transient bulk concentration available at the interface, the maximum surface tension in the loop increases as well as the minimum surface tension decreases. Furthermore an increase of the hysteresis is observed. Our simulations confirm the findings of Morris et al., who were the first to simulate the influence of the diffusion process in the bulk phase on the dynamic cycling based on a one-dimensional model.

[Figure 7 about here.]

### 5.2. Drop in shear flow

We consider a circular drop in a shear flow with  $\rho_a = \rho_w = 1000 \text{ kg/m}^3$  and  $\lambda = \eta_a/\eta_w = 0.01$ . Initially we assume the interface to be clean of any surfactant and keep the surface tension coefficient constant during the whole calculation. The drop of size  $R_0 = 1 \cdot 10^{-3} \text{ m}$  is located in the middle of a periodic rectangular channel of size  $l_x = l_y = 8R_0$  with a wall velocity of  $\pm u_\infty$ . In this case, the capillary number  $Ca$  and the Reynolds number  $Re$  are redefined by the shear rate  $G = 2u_\infty/l_y$ , i.e.

$$Ca = \frac{G\eta R}{\alpha}, \quad Re = \frac{\rho GR^2}{\eta}. \quad (36)$$

Caused by the flow shear, the drop deforms to an ellipsoid balancing the viscous stresses and surface tension. As a measure of deformation the parameter  $D = (a - b)/(a + b)$  is used, which is a ratio of the drop's length  $a$  and width  $b$ .

[Figure 8 about here.]

Fig. 8(a) shows a snapshot of the simulation when  $Ca = 0.1$  and  $Re = 1.0$ . The calculation was performed with a non-dimensional smoothing length  $h = 0.25$ , i.e. a total of 9216 particles. The deformation parameter is calculated with the least-square ellipse fitting method of Fitzgibbon et al. [26] using the interface particles to denote the shape of the droplet. A comparison of the current calculated deformations and the analytic predictions using the small-deformation theory suggested by Taylor [27] is plotted in Fig. 8(b). Even though we slightly overpredict the deformation, the agreement is good. Comparable results are presented in Hu and Adams [1], who simulated the same case but with a higher viscosity ratio of one.

[Figure 9 about here.]

Starting from the clean drop in a shear flow as a reference simulation, we consider now an initially circular droplet in the presence of an insoluble surfactant on the interface. That means that the bulk surfactant concentration in the two

phases vanishes everywhere for the entire simulation time and the interfacial surfactant mass is distributed only over the particles within the transition band at the interface. The constitutive equation for the surface-tension coefficient  $\alpha$  as function of the surfactant concentration  $\Gamma$  reduces in this example to

$$\alpha = \alpha_0 \left( 1 - \beta \frac{\Gamma}{\Gamma^*} \right), \quad (37)$$

where  $\beta$  is a parameter. Figures 9(a) and 9(b) show the deformed interface and the velocity-vector plot at steady-state for the case without surfactant ( $\beta = 0$ ) and with insoluble surfactant ( $\beta = 0.5, Pe = 1$ ) at  $Re = 1, Ca = 0.1$  and  $\lambda = 0.01$ . The deformation parameters for the two cases are calculated to be  $D = 0.107$  and  $D = 0.130$ .

Considering an insoluble surfactant present on the interface, we observe an increase of the bubble deformation of about 20%. The bubble inclination angle with respect to the x-axis at steady-state decreases slightly. The parameters in eq. (37) are chosen such that initially the surfactant concentration and the surface tension for both the clean drop and the insoluble case are the same. To study in more detail the influence of surfactants present on the interface of a shearing drop, we consider the tangential velocity along the interface and the surfactant profile. Figure 10 shows these distributions against the polar angle  $\phi$  measured around the drop's transverse diameter for the three simulated cases of a clean interface ( $\beta = 0$ ), a low diffusive ( $\beta = 0.5, Pe = 1.0$ ) and a high diffusive ( $\beta = 0.5, Pe = 0.1$ ) surfactant on the interface.

[Figure 10 about here.]

The distribution of the surfactant concentration at steady-state forms two local maxima at the tips of the deformed drop, see Fig. 10(b). With lower Peclet numbers ( $Pe = 0.1$ ) surface diffusion of the surfactant becomes more dominant and produces a nearly constant profile. Hence, the drop deformation and tangential velocity converge to the clean interface results in the limit of an infinite surface diffusion.

Contrary to Lee and Pozrikidis [17], we do not observe any region where the tangential velocity of the clean interface is negative, see Fig. 10(a). The drop rotates continuously in clockwise direction with a maximum nondimensional tangential velocity of approximately one (nondimensionalized with  $u_{ref} = GR$ ). Including surfactant effects with  $Pe = 1$ , the oscillations of the tangential velocity around  $GR/2$  decrease. Comparing the velocity vector plots in Fig. 9 shows how the diffusive surfactant on the interface affects the flow field within the droplet and in the bulk phase. The drop with the contaminated interface rotates more like a rigid body with a continuous nearly uniform tangential velocity, which is in agreement with the results of the surfactant enriched drop in a shear flow presented in [17].

From a Lagrangian point of view it is easy to explain, that the interface of a surfactant enriched insoluble drop in a shear flow at steady-state necessarily has to rotate continuously in one direction. Assuming that there are regions on the interface where the tangential velocity is negative, particles would move towards these stagnation points. As an example for such a flow situation we refer to Lee and Pozrikidis [17] (Fig. 8 and 9), who showed the streamline pattern for a clean drop in a shear flow with four stagnation points. As a consequence, particles would leave the interface

band at these regions. Without diffusion, the insoluble surfactant is transported along the interface only by advection. Whenever a particle leaves the interface region, the insoluble surfactant must stay on the interface. Hence, finally all surfactant would be concentrated at the point where the particles leave the interface region. Since this singularity is incompatible with a stable drop or ellipsoid, this flow pattern cannot exist when the interface contains insoluble surfactant.

### 5.3. Marangoni-force driven motion

Now we test our method for the Marangoni-force driven motion of a bubble. Thus, we consider a bubble with the initially non-uniform distributed surfactant concentration on the interface given by  $\Gamma = \Gamma_0 (1 + \tanh(4(\Theta/\pi - 0.5)))$ . The density and viscosity ratio of the initially quiescent bubble and bulk phase are both  $\rho_1/\rho_2 = \lambda = 1$ . The diffusion coefficient  $D_s$  is set to zero, i.e. the Peclet number is infinite. A similar test case but in three dimensions and with a different density and viscosity ratio is presented in Zhang et al. [12].

[Figure 11 about here.]

According to eq. (37) and the variation of surfactant along the interface, the interfacial surface tension gradient  $\nabla_s \alpha$  is non-zero and produces a motion of the bubble caused by the Marangoni effect. Interfacial particles at low surface tension are forced to advect towards regions of higher surface tension smoothing out the surfactant concentration distribution. On the left side of Fig. 11(a) the initial interface position and the final steady-state location of the bubble particles are shown. As the bottom part of the bubble contains initially more surfactant, the Marangoni force induced motion along the interface produces a counterclockwise rotation in the bubble phase and thus moves down. The vector plot of the velocities of the particles within the bubble (see right plot in Fig. 11(a)) shows the counterclockwise rotation of the interface and the downward motion of the drop center. The corresponding surfactant profiles along the interface during the bubble motion are shown in Fig. 11(b). The surfactant is transported along the interface by advection resulting in lowering the maximum concentration and producing an uniform profile. Hence, the surface tension finally is constant over the interface and the bubble rests at a steady position.

## 6. Concluding remarks

We have developed a fully Lagrangian particle method for simulating incompressible interfacial flows with surfactant dynamics. The surfactant transport model accounts for exchange between the bulk phase and the interface (adsorption, desorption, squeeze-out) as well as diffusion on the interface and within the bulk phase. In our numerical scheme, the different transportation phenomena can be considered simultaneously or separately, depending on the problem statement. In the present model the mass of surfactant is conserved exactly in the fluid phases and on interfaces. We have shown the validity of our method by several convergence studies and have performed several more complex simulations demonstrating the capabilities of this grid-free method. In this work we have only presented



results of two-dimensional examples. The extension of the SPH model for three-dimensional flows along the lines given in this paper is straightforward.

## 7. Acknowledgments

The authors wish to acknowledge the support of the German Research Foundation (DFG - Deutsche Forschungsgesellschaft) for funding this work within the project AD 186/6.

### A. Appendix A

To ensure exact conservation of surfactant mass in the system, we must treat the particles  $k$  that leave the interface transition band in a special way. Their fraction of interfacial mass of surfactant  $m_{sk}$  is mapped back to a particle  $i$  that remains within the transition band by

$$\Delta m_{si}^{map} = \sum_k m_{sk} \frac{W_{ki}}{\sum_l W_{kl}}, \quad (38)$$

where the smoothing function  $W_{ki}$  serves as weighting factor. To satisfy the consistency condition, this weight is normalized with  $\sum_l W_{kl}$ . Here, the summation is on all particles  $l$  of the intersection of  $k$ 's neighbors and the remaining interface particles.

### B. Appendix B

The mass exchange between an interface particle  $k$  (of an insoluble phase) and a bulk particle  $i$  (of the opposite soluble phase) is represented as

$$\Delta \left( \frac{dM_{si}}{dt} \right) = - \sum_k \dot{S}_{\Gamma_k} A_k \frac{A_i}{\sum_l A_l}, \quad (39)$$

where the fraction of the interface area  $A_i$  is used as weight. For consistency this weight is normalized with the sum of the fractions of the interface areas  $\sum_l A_l$ . Here, the summation is on all particles  $l$ , which are in the surfactant soluble phase and in the neighborhood of particle  $k$  (within the support domain of the kernel function).

### C. Appendix C

Within the weakly-compressible SPH formulation, following [22], [23] and [1] the time-step must satisfy the CFL-condition (Courant-Friedrichs-Lewy condition) based on the maximum artificial sound speed and the maximum flow speed

$$\Delta t \leq 0.25 \frac{h}{c_{max} + |u_{max}|}, \quad (40)$$

the viscous condition

$$\Delta t \leq 0.125 \frac{h^2}{\nu}, \quad (41)$$

the body force condition

$$\Delta t \leq 0.25 \left( \frac{h}{|\mathbf{g}|} \right)^{1/2}, \quad (42)$$

the surface tension condition

$$\Delta t \leq 0.25 \left( \frac{\rho h^3}{2\pi\alpha} \right)^{1/2} \quad (43)$$

and the diffusion condition

$$\Delta t \leq 0.125 \frac{h^2}{D}. \quad (44)$$

## References

- [1] X. Y. Hu, N. A. Adams, A multi-phase SPH method for macroscopic and mesoscopic flows, *Journal of Computational Physics* 213 (2) (2006) 844–861.
- [2] R. E. Pattle, Properties, function and origin of the alveolar lining layer, *Nature* 175 (4469) (1955) 1125–1126.
- [3] J. Clements, Surface tension of lung extracts., *Proc Soc Exp Biol Med* 95 (1957) 170–172.
- [4] K. Von Neergard, Neue Auffassung über einen Grundbegriff der Atemmechanik, *Z Ges Exp Med* 66 (1929) 373–393.
- [5] H. Hamm, H. Fabel, W. Bartsch, The surfactant system of the adult lung - physiology and clinical perspectives.
- [6] H. A. Stone, L. G. Leal, The effects of surfactants on drop deformation and breakup, *Journal of Fluid Mechanics* 220 (1990) 161–186.
- [7] S. Yon, C. Pozrikidis, A finite-volume/boundary-element method for flow past interfaces in the presence of surfactants, with application to shear flow past a viscous drop, *Computers & Fluids* 27 (8) (1998) 879–902.
- [8] J.-J. Xu, H.-K. Zhao, An eulerian formulation for solving partial differential equations along a moving interface, *Journal of Scientific Computing* 19 (1) (2003) 573–594.
- [9] A. J. James, J. Lowengrub, A surfactant-conserving volume-of-fluid method for interfacial flows with insoluble surfactant, *J. Comput. Phys.* 201 (2) (2004) 685–722.
- [10] J.-J. Xu, Z. Li, J. Lowengrub, H. Zhao, A level-set method for interfacial flows with surfactant, *Journal of Computational Physics* 212 (2) (2006) 590–616.
- [11] M.-C. Lai, Y.-H. Tseng, H. Huang, An immersed boundary method for interfacial flows with insoluble surfactant, *Journal of Computational Physics* 227 (15) (2008) 7279–7293.
- [12] J. Zhang, D. Eckmann, P. Ayyaswamy, A front tracking method for a deformable intravascular bubble in a tube with soluble surfactant transport, *Journal of Computational Physics* 214 (1) (2006) 366–396.
- [13] M. Muradoglu, G. Tryggvason, A front-tracking method for computation of interfacial flows with soluble surfactants, *Journal of Computational Physics* 227 (4) (2008) 2238–2262.

- [14] J. P. Morris, P. J. Fox, Y. Zhu, Modeling low reynolds number incompressible flows using SPH, *Journal of Computational Physics* 136 (1) (1997) 214–226.
- [15] R. P. Borwankar, D. T. Wasan, The kinetics of adsorption of surface active agents at gas-liquid surfaces, *Chemical Engineering Science* 38 (10) (1983) 1637–1649.
- [16] D. R. Otis, E. P. Ingenito, R. D. Kamm, M. Johnson, Dynamic surface tension of surfactant TA: experiments and theory, *Journal of Applied Physiology* 77 (6) (1994) 2681–2688.
- [17] J. Lee, C. Pozrikidis, Effect of surfactants on the deformation of drops and bubbles in Navier-Stokes flow, *Computers & Fluids* 35 (1) (2006) 43–60.
- [18] G. Tryggvason, B. Bunner, A. Esmaeeli, D. Juric, N. Al-Rawahi, W. Tauber, J. Han, S. Nas, Y. J. Jan, A front-tracking method for the computations of multiphase flow, *Journal of Computational Physics* 169 (2) (2001) 708–759.
- [19] M. Bertalmío, L.-T. Cheng, S. Osher, G. Sapiro, Variational problems and partial differential equations on implicit surfaces, *Journal of Computational Physics* 174 (2) (2001) 759–780.
- [20] J. K. Chen, J. E. Beraun, T. C. Carney, A corrective smoothed particle method for boundary value problems in heat conduction, *International Journal for Numerical Methods in Engineering* 46 (2) (1999) 231–252.
- [21] I. F. Sbalzarini, A. Hayer, A. Helenius, P. Koumoutsakos, Simulations of (an)isotropic diffusion on curved biological surfaces, *Biophys. J.* 90 (3) (2006) 878–885.
- [22] J. J. Monaghan, Smoothed particle hydrodynamics, *Reports in Progress in Physics* 68 (8) (2005) 1703–1759.
- [23] Y. Zhu, P. J. Fox, Smoothed particle hydrodynamics model for diffusion through porous media, *Transport in Porous Media* 43 (3) (2001) 441–471.
- [24] J. Morris, E. Ingenito, L. Mark, R. Kamm, M. Johnson, Dynamic behavior of lung surfactant, *Journal of Biomechanical Engineering* 123 (2001) 106–113.
- [25] S. Schurch, D. Schurch, T. Curstedt, B. Robertson, Surface activity of lipid extract surfactant in relation to film area compression and collapse, *J Appl Physiol* 77 (2) (1994) 974–986.
- [26] A. Fitzgibbon, M. Pilu, R. B. Fisher, Direct least square fitting of ellipses, *IEEE Transactions on Pattern Analysis and Machine Intelligence* 21 (1999) 476–480.
- [27] G. I. Taylor, The formation of emulsions in definable fields of flow, *Proceedings of the Royal Society of London. Series A, Containing Papers of a Mathematical and Physical Character* (1905-1934) 146 (858) (1934) 501–523.

## List of Figures

1	Sketch of the transition band at an interface with the surface delta function $\delta_\Sigma$ and particles of two different phases. . . . .	21
2	(a) Concentration profiles of bulk diffusion at $t = 0.0, 1.5$ and $3.0$ ; solid line: analytic solution, symbols: SPH results. (b) $L_1$ error with respect to smoothing length $h$ for the bulk diffusion test (see Sec. 4.1). . . . .	22
3	(a) Concentration profiles of interfacial diffusion at $t = 0, 0.5, 1.0$ and $2.0$ ; solid line: analytic solution, symbols: SPH results. (b) $L_1$ error with respect to smoothing length $h$ for the interfacial diffusion test (see Sec. 4.2). . . . .	23
4	(a) Non-dimensional surfactant concentration profile at $t = 5$ with $D_n = 1 \cdot 10^{-6} m^2/s$ and $h = 0.125$ for the two normal formulations (curves are shifted for clarity). (b) Comparison of interface normals formulation; left: Calculation with $\mathbf{n}_i = \nabla c_i /  \nabla c_i $ , right: Calculation with eq. (27). . . . .	24
5	(a) Surfactant transport to a steady interface, comparison between adsorption-limited $D_\infty = \infty$ and diffusion-limited $D_\infty = 10^{-6} m^2/s$ case. (b) Mass of surfactant on the interface and in the liquid phase over time. . . . .	25
6	Stationary surface tension loops. (a) $Bi = 1, \tilde{k} = 1, 10$ and $100$ (b) $\tilde{k} = 10, Bi = 0.1, 1$ and $10$ . . . . .	26
7	Comparison between the adsorption-limited ( $D \rightarrow \infty$ ) and the diffusion-limited model ( $D = 4 \cdot 10^{-3} m^2/s$ ). (a) Evolution of the surfactant concentration in the bulk subsurface region directly underneath the interface. (b) Corresponding surface-tension loops. . . . .	27
8	(a) Positions of air particles (black dots) and shearing water particles (open circles) for $Ca = 0.1, Re = 1.0$ and $\lambda = 0.01$ (b) Drop deformation parameter $D$ over capillary number $Ca$ for $\lambda = 0.01$ . . . . .	28
9	Interface position and velocity vector plot of a drop in a shear flow at $Re = 1, \lambda = 0.01$ and $Ca = 0.1$ . (a) Clean droplet ( $\beta = 0.0$ ). (b) Insoluble surfactant on the interface ( $\beta = 0.5, Pe = 1$ ). . . . .	29
10	Effect of surfactant on the steady deformation of a drop in a shear flow at $Re = 1, \lambda = 0.01$ and $Ca = 0.1$ . (a) Distribution of tangential velocity for the cases $\beta = 0., \beta = 0.5, Pe = 0.1$ and $\beta = 0.5, Pe = 1.0$ . (b) Distribution of the interfacial surfactant concentration for $Pe = 0.1$ and $Pe = 1$ . . . . .	30
11	Interface positions (left) and velocity field (right) for an initially non-uniform surfactant covered bubble moving due to the Marangoni effect. . . . .	31

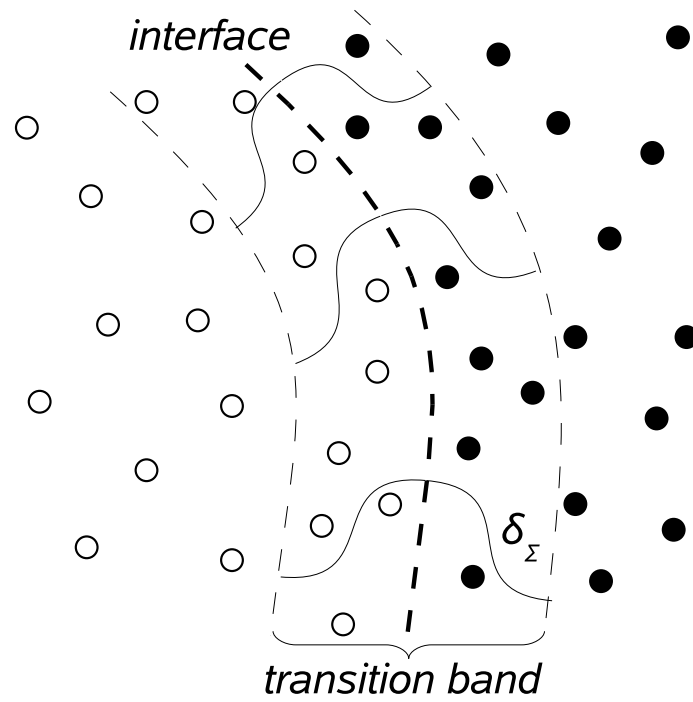


Figure 1: Sketch of the transition band at an interface with the surface delta function  $\delta_\Sigma$  and particles of two different phases.

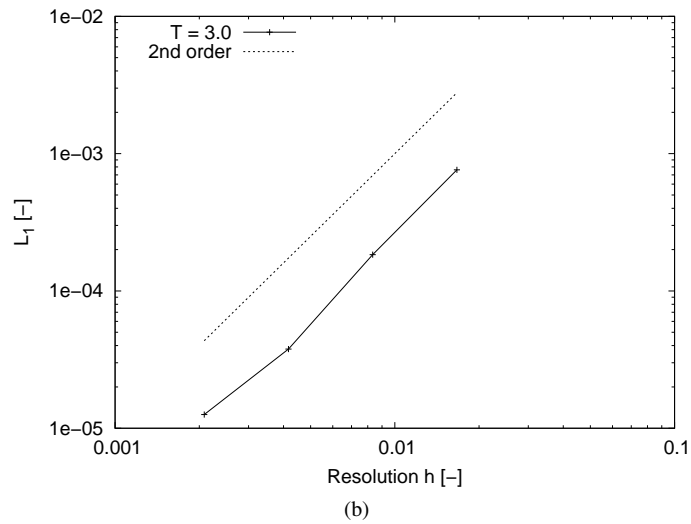
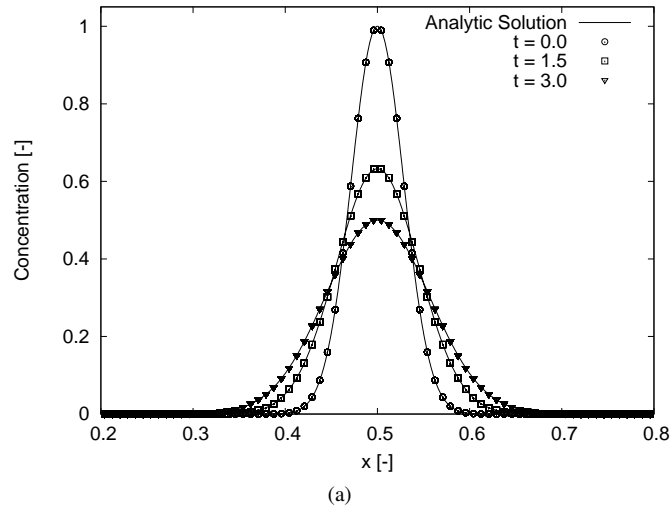


Figure 2: (a) Concentration profiles of bulk diffusion at  $t = 0.0, 1.5$  and  $3.0$ ; solid line: analytic solution, symbols: SPH results. (b)  $L_1$  error with respect to smoothing length  $h$  for the bulk diffusion test (see Sec. 4.1).

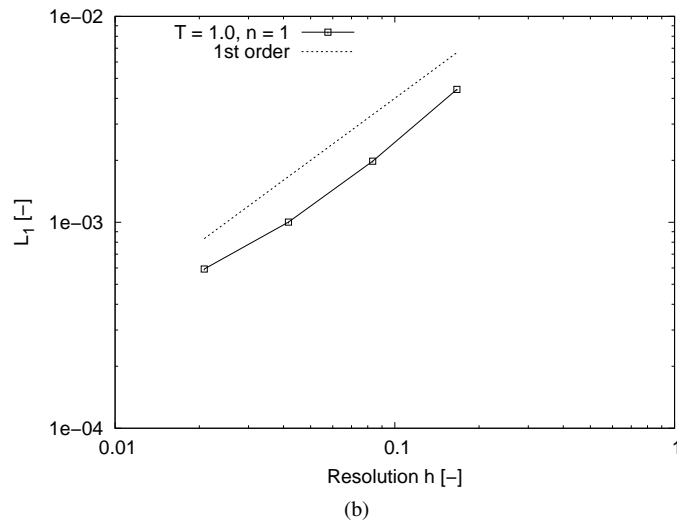
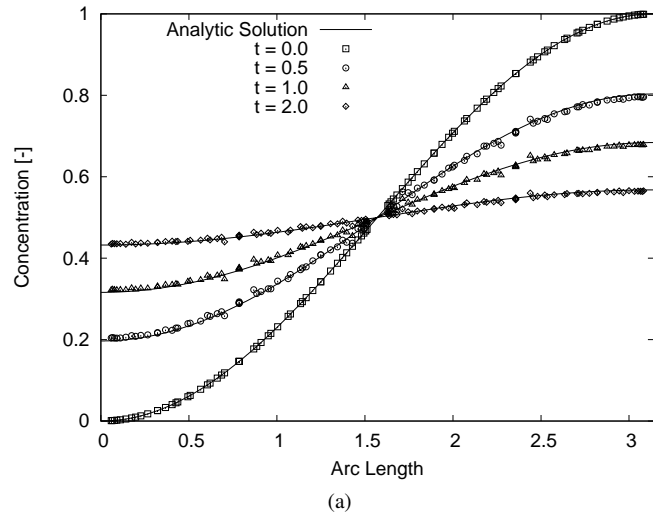
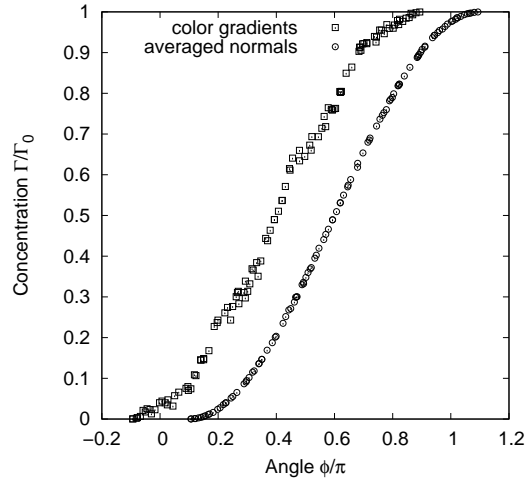
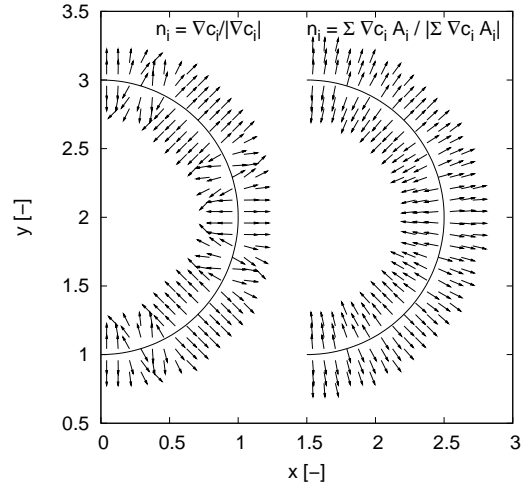


Figure 3: (a) Concentration profiles of interfacial diffusion at  $t = 0, 0.5, 1.0$  and  $2.0$ ; solid line: analytic solution, symbols: SPH results. (b)  $L_1$  error with respect to smoothing length  $h$  for the interfacial diffusion test (see Sec. 4.2).



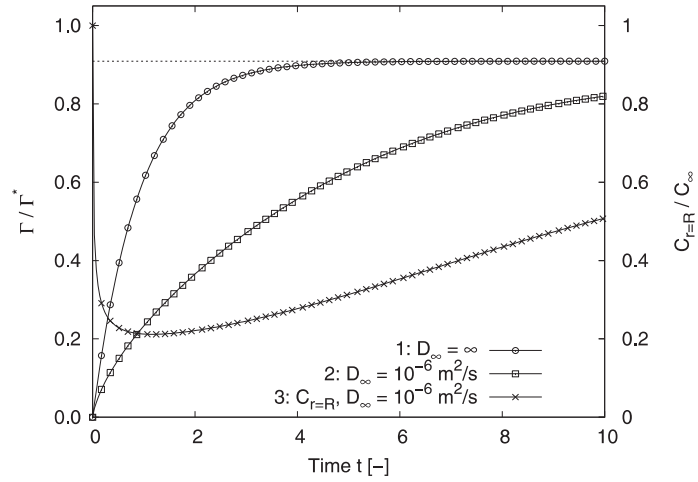
(a)



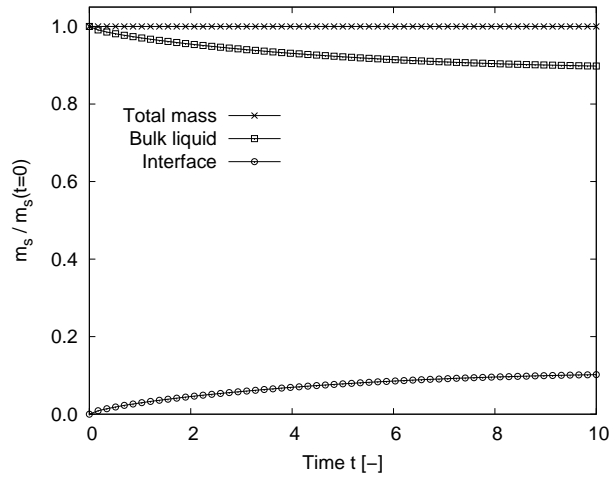
(b)

Figure 4: (a) Non-dimensional surfactant concentration profile at  $t = 5$  with  $D_n = 1 \cdot 10^{-6} \text{ m}^2/\text{s}$  and  $h = 0.125$  for the two normal formulations (curves are shifted for clarity). (b) Comparison of interface normals formulation; left: Calculation with  $\mathbf{n}_i = \nabla c_i / |\nabla c_i|$ , right: Calculation with eq. (27).



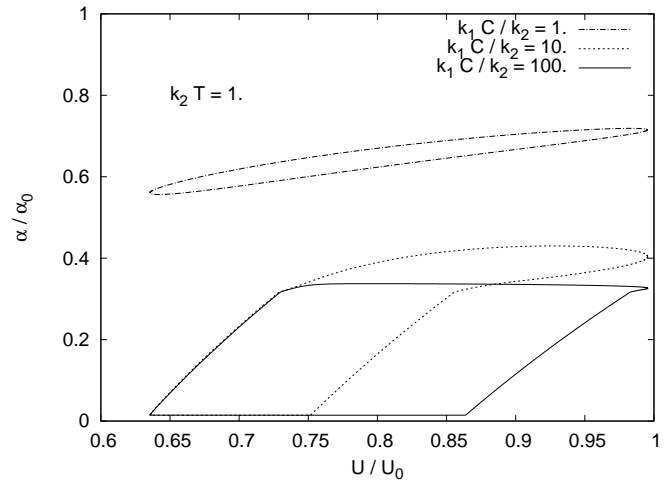


(a)

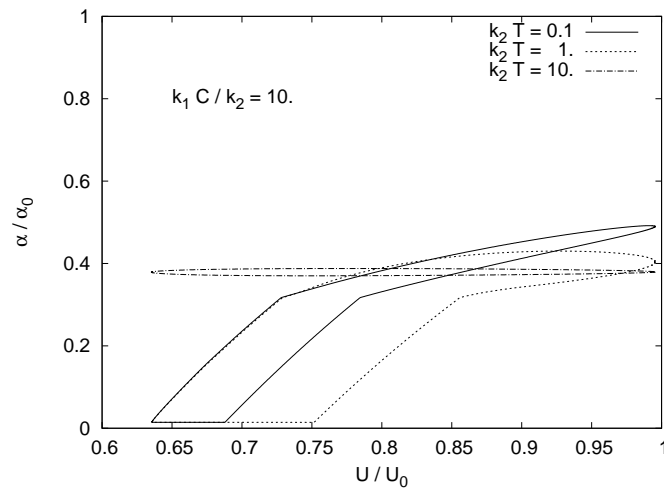


(b)

Figure 5: (a) Surfactant transport to a steady interface, comparison between adsorption-limited  $D_{\infty} = \infty$  and diffusion-limited  $D_{\infty} = 10^{-6} m^2/s$  case. (b) Mass of surfactant on the interface and in the liquid phase over time.

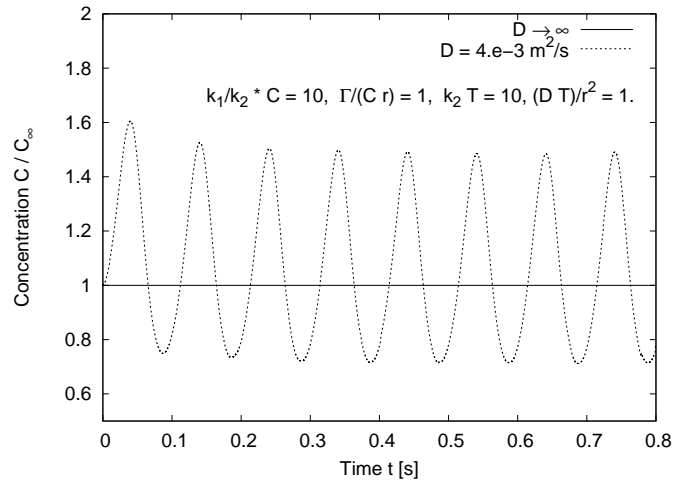


(a)

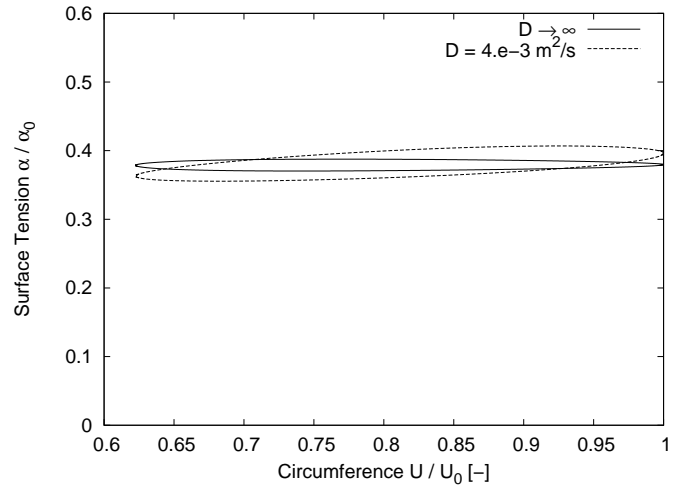


(b)

Figure 6: Stationary surface tension loops. (a)  $Bi = 1$ ,  $\tilde{k} = 1, 10$  and  $100$  (b)  $\tilde{k} = 10$ ,  $Bi = 0.1, 1$  and  $10$



(a)



(b)

Figure 7: Comparison between the adsorption-limited ( $D \rightarrow \infty$ ) and the diffusion-limited model ( $D = 4 \cdot 10^{-3} m^2/s$ ). (a) Evolution of the surfactant concentration in the bulk subsurface region directly underneath the interface. (b) Corresponding surface-tension loops.

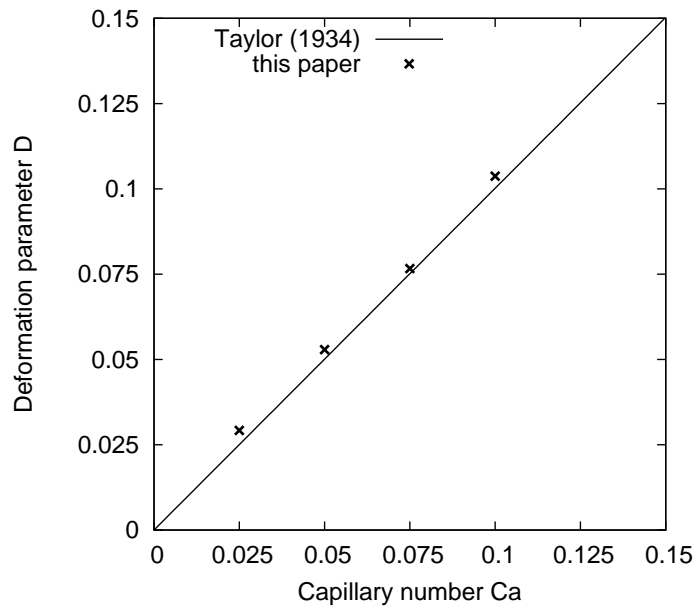
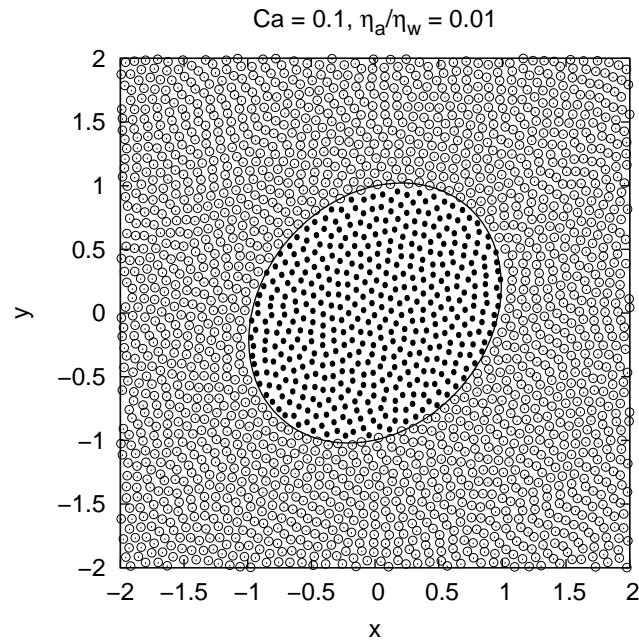
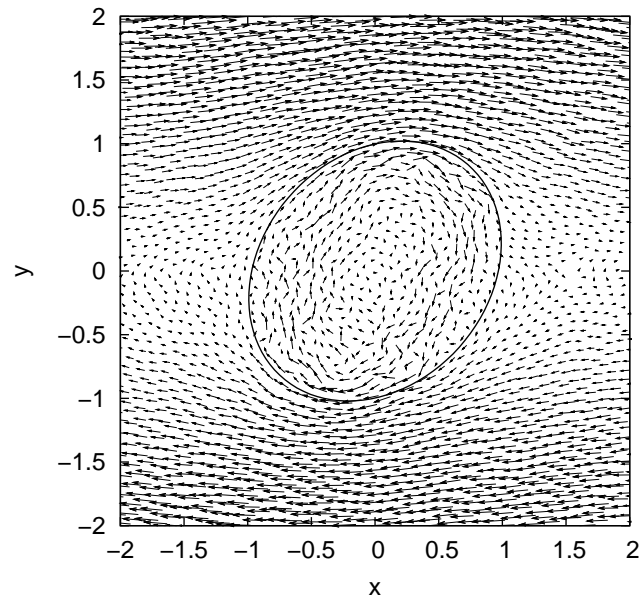
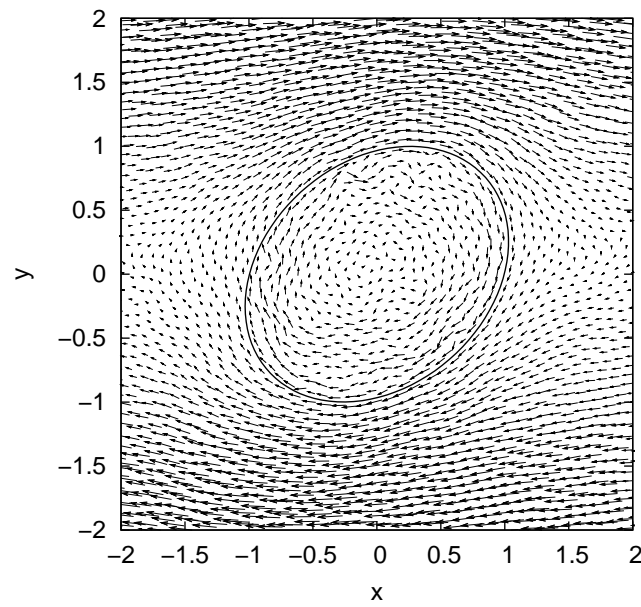


Figure 8: (a) Positions of air particles (black dots) and shearing water particles (open circles) for  $Ca = 0.1$ ,  $Re = 1.0$  and  $\lambda = 0.01$  (b) Drop deformation parameter  $D$  over capillary number  $Ca$  for  $\lambda = 0.01$ .

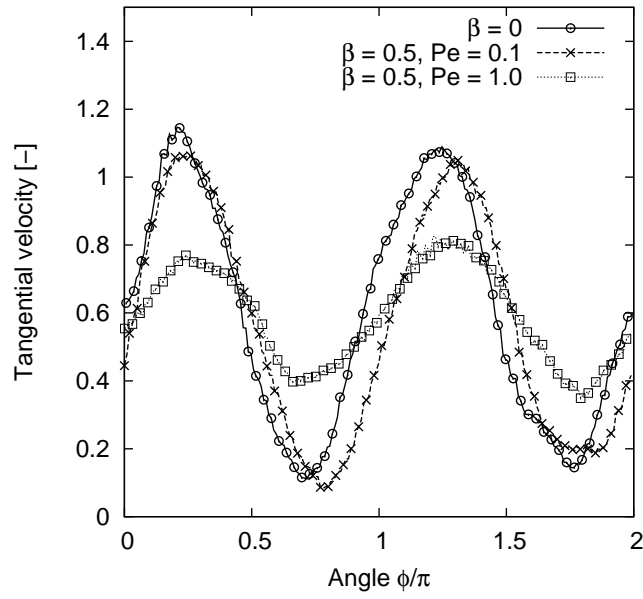


(a)

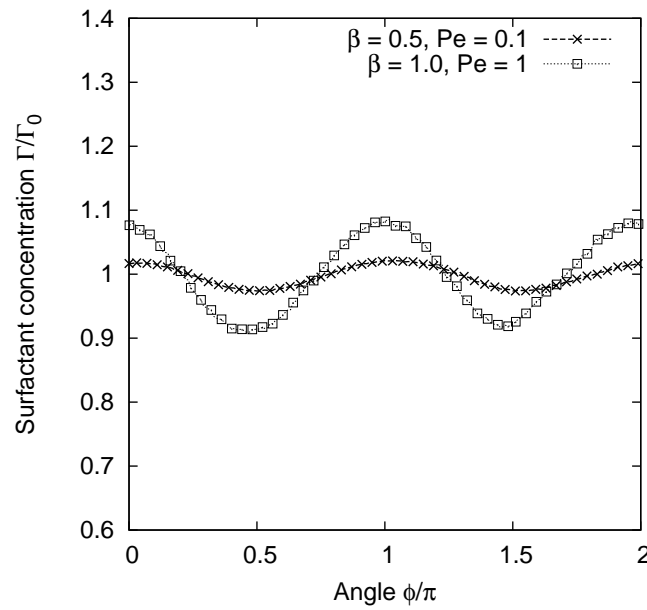


(b)

Figure 9: Interface position and velocity vector plot of a drop in a shear flow at  $Re = 1$ ,  $\lambda = 0.01$  and  $Ca = 0.1$ . (a) Clean droplet ( $\beta = 0.0$ ). (b) Insoluble surfactant on the interface ( $\beta = 0.5$ ,  $Pe = 1$ ).

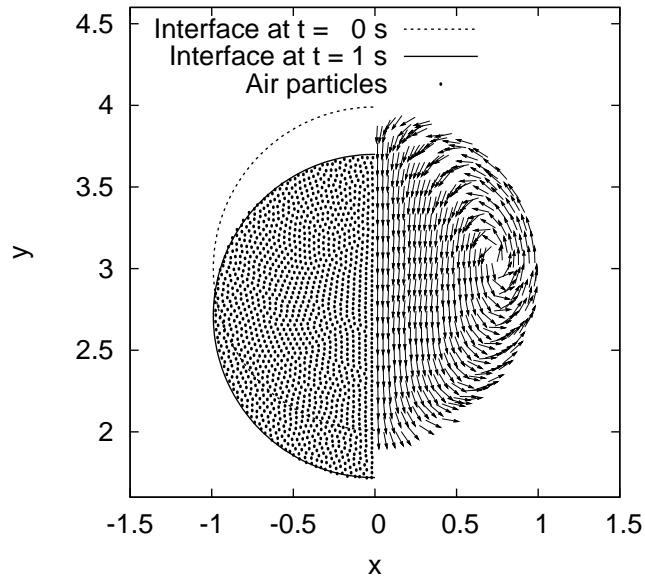


(a)

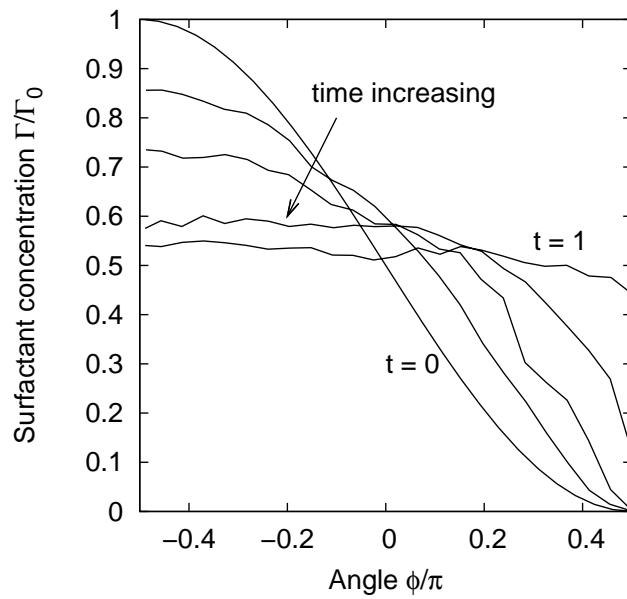


(b)

Figure 10: Effect of surfactant on the steady deformation of a drop in a shear flow at  $Re = 1$ ,  $\lambda = 0.01$  and  $Ca = 0.1$ . (a) Distribution of tangential velocity for the cases  $\beta = 0.$ ,  $\beta = 0.5$ ,  $Pe = 0.1$  and  $\beta = 0.5$ ,  $Pe = 1.0$ . (b) Distribution of the interfacial surfactant concentration for  $Pe = 0.1$  and  $Pe = 1$ .



(a)



(b)

Figure 11: Interface positions (left) and velocity field (right) for an initially non-uniform surfactant covered bubble moving due to the Marangoni effect.